Available online at www.CivileJournal.org

Civil Engineering Journal

(E-ISSN: 2476-3055; ISSN: 2676-6957)

Vol. 10, No. 05, May, 2024

Influence of Shear Strain on the Deflection of Girders

Antonia J. Lazarević [1*], Tanja Mališ [1], Elizabeta Šamec [2], Elizabeta Jerečić [1]

[1] *Faculty of Mining, Geology and Petroleum Engineering, University of Zagreb, Pierottijeva 6, HR-10000 Zagreb, Croatia.*

[2] *Faculty of Civil Engineering, University of Zagreb, Fra Andrije Kačića-Miošića 26, HR-10000 Zagreb, Croatia.*

Received 02 February 2024; Revised 22 April 2024; Accepted 27 April 2024; Published 01 May 2024

Abstract

Numerical calculations are a standard part of modern structural design. Engineers remain particularly interested in real problems where analytical and numerical solutions can be compared with experimental results. Such cases are typical examples of benchmarks because they are used to verify the assumptions introduced. This study shows in detail how shear stresses affect the deflection of a relatively short and high cantilever when the span-to-height ratio of the cross-section is less than five. Such models are frequently used in the design of cantilevers that support heavily loaded beams, for example in the cement industry (e.g., often as structural elements for a heat exchanger system) or for the assessment of short cantilever limit states that appear during excavation in rock sediments. The models are also suitable for designing the various details and joints in the industry of prefabricated elements. This work analyzes in depth the analytical solutions for the displacement field of the linear elastic plane stress theory with two displacement boundary conditions. Also, the solutions were compared with the beam, two-, and three-dimensional numerical models using SAP2000. The results highlight the fundamental principles and solutions behind plane stress and beam theories, with an insight into the advantages and limitations of such models.

Keywords: Short Cantilever; Linear Elasticity Theory; Analytical Solution of the Displacement Field; Plane Stress State; SAP2000.

1. Introduction

Selecting a mathematical model to predict the behavior of a real deformable body is a fundamental step in engineering calculations. A set of necessary approximations required for the creation of a numerical model; its mathematical counterpart should be based on unavoidable errors. Thus, creating a good model involves simplifying it as much as possible while still getting reliable and clear results [1–3]. The most common problems engineers come across in the mechanics of solid bodies are solved within the framework of linear elasticity. The adoption of material and geometric linearization of the continuum results in a mathematical formulation represented by 15 partial differential equations: six kinematic equations, three equilibrium conditions, and six constitutive equations. For a particular body shape and boundary conditions, the system is solved using the force method, displacement method, or a mixed approach, and a solution is obtained for the fields of displacements, strains, and stresses, depending on the choice of the solution strategy [4, 5]. As this is a very complex system of equations, an analytical solution can only be found for a very few practical problems.

Since a closed-form solution is rarely possible, additional simplifications of the body's geometry, load, and boundary conditions are frequently used. For such purposes, engineers use so-called submodels such as beams, plates, shells, plane stress, or strain states. When choosing a submodel, it is crucial to recognize the essential characteristics of the corresponding mathematical model, which are important for the accuracy of the results [6–8]. Although represented by

* Corresponding author: antonia.jaguljnjak-lazarevic@rgn.unizg.hr

http://dx.doi.org/10.28991/CEJ-2024-010-05-04

a simpler mathematical formulation, many useful submodels lack an analytical solution, or the manual calculation procedure is too complex. In this case, numerical strategies are utilized at the cost of additional approximations, such as continuum discretization techniques supported by numerical methods. Nevertheless, these approximations can lead to an estimated error of up to 30% when modeling a typical engineering problem for static loads [9, 10].

Although computational procedures are a standard approach in the design of structures, engineers are still particularly interested in real problems where analytical and numerical solutions can be compared with experimental results. Such examples are known as benchmarks because they are used to verify the assumptions made during the design process [11].

This study demonstrated the creation of an analytical solution for a relatively short and high cantilever, where the ratio of span L to the cross-sectional height h was less than five. When analyzing such a model, the Euler-Bernoulli-Navier hypothesis (EBN - the cross-sections remain plain) cannot be applied; therefore, the influence of the shear stresses (integral shear force) on the deflection must be considered. For the EBN theory to be valid, the ratio of $L/h > 5$ is commonly used for engineering structures [12]; however, the limit may be stricter depending on the type of material [5]. For example, according to some authors [13], to apply the EBN hypothesis in rock mechanics, the ratio of span to height must be $L/h > 8$. The standard for determining the flexural strength of natural stone, "HR EN 12372", also stipulates the ratio of $L/h > 6$.

Interestingly, although the original EBN and Timoshenko beam theories are rather old, they still intrigue researchers in the various fields of theoretical mechanics and computational methods [14-16]. Also, novel approaches, formulations, and extensions are growing constantly [17-19]. The practical application of both theories is continually present [20, 21].

Figure 1 shows the process and methodology of the work: the description and definition of the problem, the determination of analytical solutions, the formulation of numerical models, and the comparison and analysis of the results.

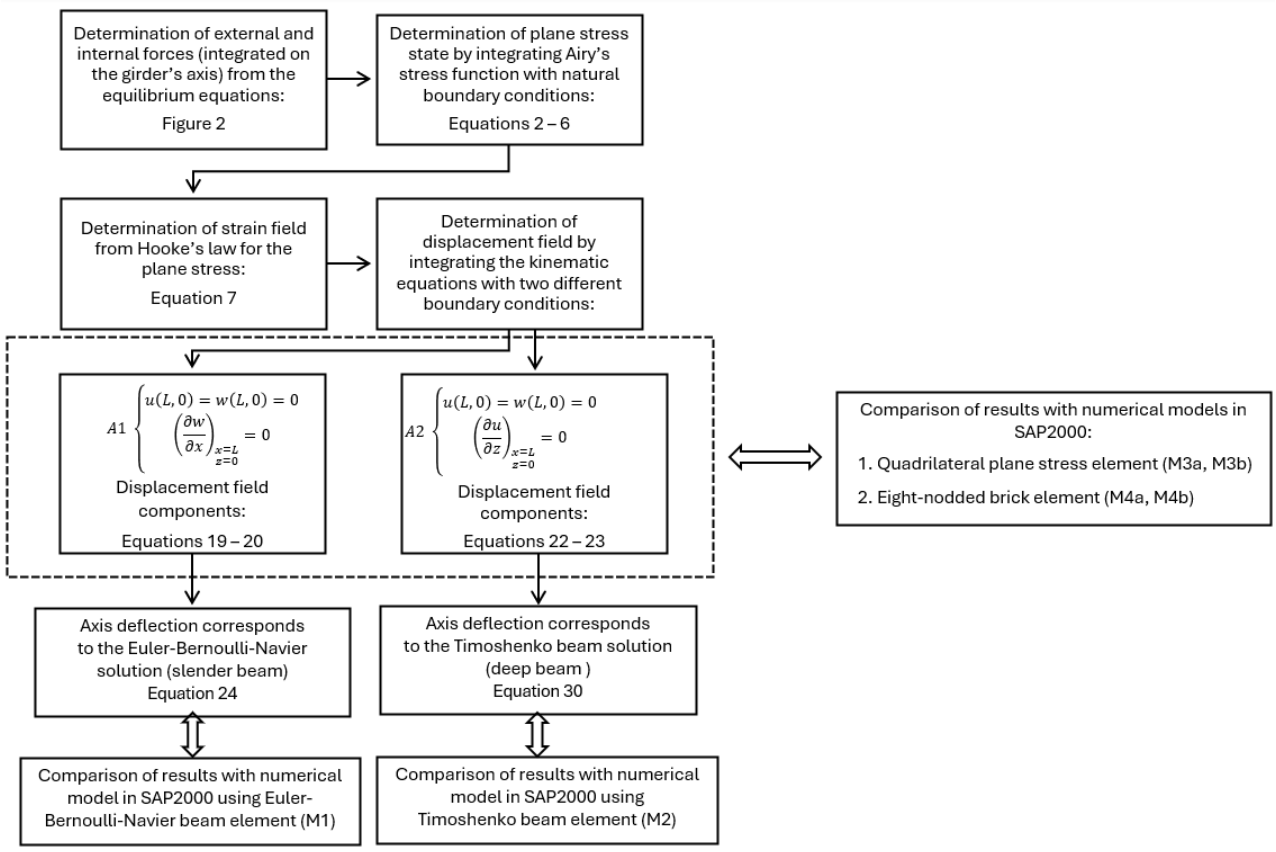

Figure 1. A flowchart that briefly explains the analysis procedure

2. Description of the Model Problem

Figure 2-a shows a right-hand cantilever of a length L loaded by a concentrated force F in the girder axis, a resultant of a continuous tangential load q_f with a parabolic distribution along the height of the free left end. Because this is a linear problem and a statically determinate system, the equilibrium equations for the undeformed system are solved independently of the constitutive and kinematic equations. Diagrams of the internal forces along the girder axis are shown in Figures 2-b and 2-c.

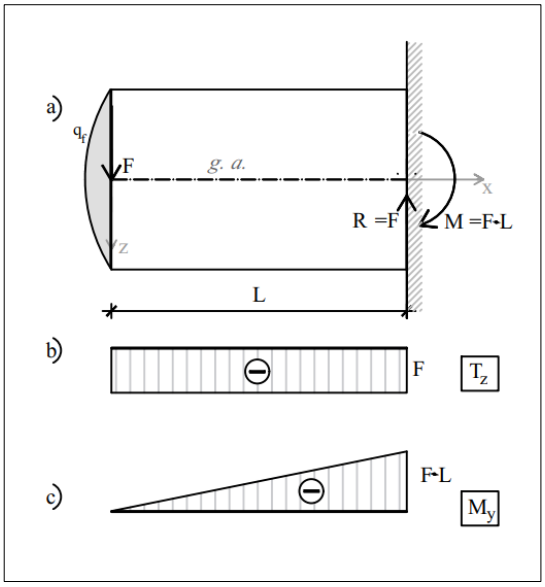

Figure 2. External and internal forces integrated on the girder's axis are a) load F, reactions R and M, b) shear forces T_z, and c) bending moments M_y

For the defined problem, we used a submodel of the girder which corresponds to the model of the plane stress. According to the formulation by the force method, the stress state for an isotropic material is described by Airy's stress function $\Phi\ (x, z)$ for which [4]:

$$\frac{\partial^4\Phi}{\partial x^4} + 2\frac{\partial^4\Phi}{\partial x^2\partial z^2} + \frac{\partial^4\Phi}{\partial z^4} = 0, \tag{1}$$

where the stress components are equal to:

$$\sigma_x = \frac{\partial^2\Phi}{\partial z^2}, \quad \sigma_z = \frac{\partial^2\Phi}{\partial x^2}, \quad \tau_{xz} = \tau_{zx} = -\frac{\partial^2\Phi}{\partial x\partial z}. \tag{2}$$

Equation 1 represents Maxwell's fourth-order elliptic partial differential equation that satisfies the equilibrium and compatibility conditions.

The solution of the stress field is obtained by integration, according to given boundary conditions. For the right-hand cantilever with rectangular cross-section and constant width, loaded at the free end with a concentrated force (Figure 3), the stress state can be determined from the set of polynomials [4] by the superposition of solutions Φ_2 and Φ_4:

$$\Phi_2 = \frac{a_2}{2}x^2 + b_2 \cdot x \cdot z + \frac{c_2}{2}z^2, \tag{3}$$

$$\Phi_4 = \frac{a_4}{4\cdot3}x^4 + \frac{b_4}{3\cdot2}x^3 \cdot z + \frac{c_4}{2}x^2 \cdot z^2 + \frac{d_4}{3\cdot2}x \cdot z^3 + \frac{e_4}{4\cdot3}z^4, \tag{4}$$

with $a_2 = c_2 = 0$ and $a_4 = b_4 = c_4 = e_4 = 0$.

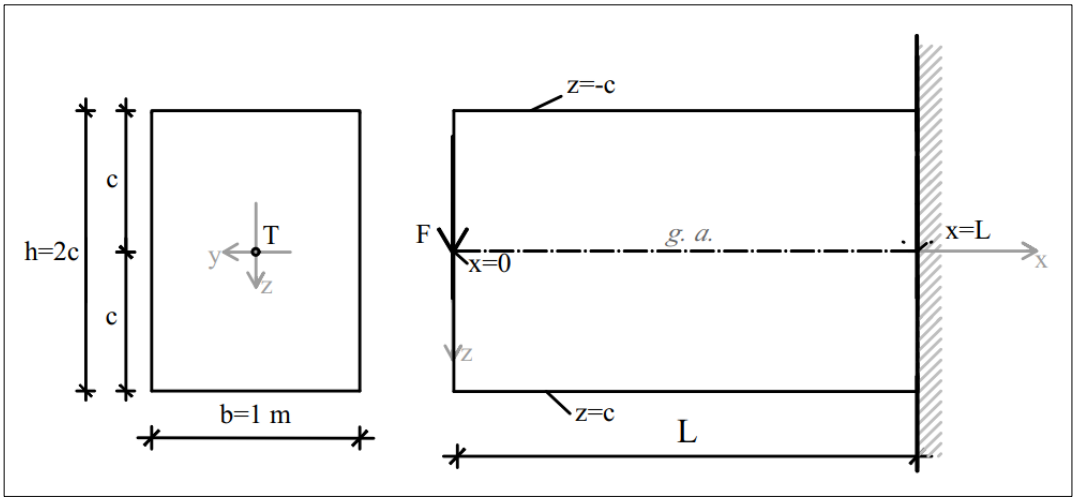

Figure 3. The geometry of the model

According to Equation 2, the plane stress state is obtained as follows:

$$\sigma_x = \frac{\partial^2 \Phi_2}{\partial z^2} + \frac{\partial^2 \Phi_4}{\partial z^2} = d_4 \cdot x \cdot z,$$
$$\sigma_z = \frac{\partial^2 \Phi_2}{\partial x^2} + \frac{\partial^2 \Phi_4}{\partial x^2} = 0, \quad (5)$$
$$\tau_{xz} = -\frac{\partial^2 \Phi_2}{\partial x \partial z} + \left(-\frac{\partial^2 \Phi_4}{\partial x \partial z}\right) = -\left(b_2 + \frac{d_4}{2} \cdot z^2\right).$$

We determined the constants b_2 i d_4 from the natural boundary conditions. At the upper (or lower) edge of the girder there are no shear stresses, $\tau_{xz} = 0$, and $\int_{-c}^{c} \tau_{xz}\, dz = T_z$ is applied along and at the ends of the girder, from which:

$$\sigma_x = -\frac{3T_z}{2c^3} \cdot x \cdot z = -\frac{T_z}{I_y} x \cdot z,$$
$$\tau_{xz} = -\frac{3T_z}{4c}\left(1 - \frac{z^2}{c^2}\right) = -\frac{T_z}{2I_y}(c^2 - z^2), \quad (6)$$

where the moment of inertia $I_y = bh^3/12$ for $b = 1$ and $h = 2c$ is $I_y = 2c^3/3$.

A graphical representation of the stress distribution in the characteristic cross-sections along the height of the girder is shown in Figure 4.

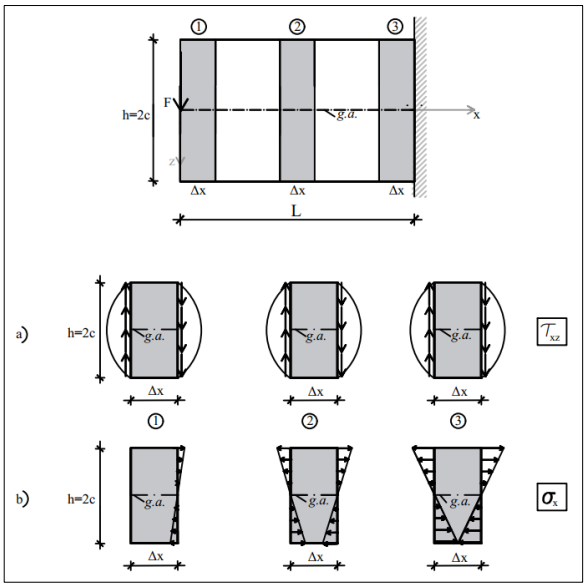

Figure 4. Stress state in the girder: a) shear stresses τ_{xz} and b) normal stresses σ_x

The shear stresses change with the height of the cross-section according to the quadratic function, whereas the stress intensities remained constant along the axis. The normal stresses are linear along the height and length of the girder. Note that the equilibrium condition of each cross-section along the z-axis is satisfied integrally by the shear stresses (Figure 4a), while the equilibrium along the x-axis is ensured by the integral of the normal stresses (Figure 4b). However, the moment around the y-axis from the shear stresses τ_{xz} is balanced by the difference in moments from the normal stresses σ_x.

For the stress state, according to Equation 6, the strain field was determined from Hooke's law for the plane stress [4]:

$$\varepsilon_x = \frac{1}{E}(\sigma_x - \nu\sigma_z) = \frac{\sigma_x}{E} = -\frac{1}{E} \cdot \frac{3T_z}{2c^3} \cdot x \cdot z = -\frac{T_z}{EI_y} \cdot x \cdot z,$$
$$\varepsilon_y = \frac{1}{E}(\sigma_z - \nu\sigma_x) = -\frac{\nu\sigma_x}{E},$$
$$\varepsilon_z = -\frac{\nu}{E}(\sigma_x - \sigma_z) = -\frac{\nu\sigma_x}{E} = \frac{\nu T_z}{EI_y} \cdot x \cdot z, \quad (7)$$
$$\gamma_{xz} = \frac{\tau_{xz}}{G} = -\frac{1}{G} \cdot \frac{3T_z}{4c}\left(1 - \frac{z^2}{c^2}\right) = -\frac{T_z}{2GI_y}(c^2 - z^2).$$

Note that the spatial strain state is obtained where the strain ε_y does not influence the deflection; thus, it does not need to be considered.

Displacements u and w were obtained by integrating the kinematic equations (relationships between strain and displacement):

$$\varepsilon_x = \frac{\partial u}{\partial x} \rightarrow u = -\frac{T_z}{2EI_y} \cdot x^2 \cdot z + p_1(z),$$
$$\varepsilon_z = \frac{\partial w}{\partial z} \rightarrow w = +\frac{\nu T_z}{2EI_y} \cdot x \cdot z^2 + p_2(x), \quad (8)$$

where $p_1(z)$ and $p_2(x)$ are unknown functions.

From the expression for shear strain $\gamma_{xz} = \partial u / \partial z + \partial w / \partial x$ we obtain:

$$-\frac{T_z}{2EI_y} \cdot x^2 + \frac{df_1}{dz} + \frac{\nu T_z}{2EI_y} \cdot z^2 + \frac{df_2}{dx} = -\frac{T_z}{2GI_y}(c^2 - z^2) \quad (9)$$

The sums of the terms in the expression above, which are functions of only one variable, x or z, are denoted by d and e:

$$d = -\frac{T_z}{2EI_y} \cdot x^2 + \frac{dp_2}{dx},$$
$$e = \frac{dp_1}{dz} + \frac{\nu T_z}{2EI_y} \cdot z^2 - \frac{T_z}{2GI_y} \cdot z^2, \quad (10)$$

Thus, Equation 9 becomes:

$$d + e = -\frac{c^2 T_z}{2GI_y} = \text{const.} \quad (11)$$

which is possible only if d and e are also constants.

By integrating Equation 10, we obtain the functions $p_1(z)$ and $p_2(x)$:

$$p_2(x) = \frac{T_z}{6EI_y} \cdot x^3 + d \cdot x + f,$$
$$p_1(z) = \frac{T_z}{6I_y}\left(\frac{1}{G} - \frac{\nu}{E}\right) \cdot z^3 + e \cdot z + g \quad (12)$$

where f and g are integration constants.

Finally, by substituting Equation 12 into Equation 8, the displacement equations are

$$u(x,z) = -\frac{T_z}{2EI_y} \cdot x^2 \cdot z + \frac{T_z}{6I_y}\left(\frac{1}{G} - \frac{\nu}{E}\right) \cdot z^3 + e \cdot z + g, \quad (13)$$

$$w(x,z) = \frac{\nu T_z}{2EI_y} \cdot x \cdot z^2 + \frac{T_z}{6EI_y} \cdot x^3 + d \cdot x + f. \quad (14)$$

The constants d (or e), g, and f result from the boundary conditions that prevent the rigid body motion of the girder and are achieved by the correct position of the supports. In our example this is clamped support, that is, the rotational, horizontal and vertical degrees of freedom at point A (0, L) are fixed.

From conditions $u_A(L, 0) = 0$ and $w_A(L, 0) = 0$ follows:

$$g = 0,$$
$$\frac{T_z}{6EI_y} \cdot L^3 + d \cdot L + f = 0 \;\Rightarrow\; f = -\frac{T_z}{6EI_y} \cdot L^3 - d \cdot L. \quad (15)$$

The angle of rotation at point A can be prevented in two ways:

$$\left(\frac{\partial w}{\partial x}\right)_{\substack{x=L \\ z=0}} = 0, \quad (16)$$

$$\left(\frac{\partial u}{\partial z}\right)_{\substack{x=L \\ z=0}} = 0, \quad (17)$$

Therefore, we consider two possible solutions for the displacement field. From the boundary conditions in Equation 16 and using Equations 11, 14, and 15, we obtain:

$$d = -\frac{T_z}{2EI_y} \cdot L^2,\; f = \frac{T_z L^3}{3EI_y},\; e = \frac{T_z}{2I_y}\left(\frac{L^2}{E} - \frac{c^2}{G}\right), \quad (18)$$

Consequently, the displacements are:

$$u(x,z) = -\frac{T_z}{2EI_y} \cdot x^2 \cdot z + \frac{T_z}{6I_y}\left(\frac{1}{G} - \frac{\upsilon}{E}\right) \cdot z^3 + \frac{T_z}{2I_y}\left(\frac{L^2}{E} - \frac{c^2}{G}\right) \cdot z, \quad (19)$$

$$w(x,z) = \frac{\nu T_z}{2EI_y} \cdot x \cdot z^2 + \frac{T_z}{6EI_y} \cdot x^3 - \frac{T_z L^2}{2EI_y} \cdot x + \frac{T_z L^3}{3EI_y}. \quad (20)$$

For the prevented angle of rotation, according to Equation 17, we obtain the following values from Equations 11, 14, and 15:

$$e = \frac{T_z L^2}{2EI_y},\ d = -\frac{T_z}{2I_y}\cdot\left(\frac{c^2}{G}+\frac{L^2}{E}\right),\ f = \frac{T_z L^3}{3EI_y}+\frac{T_z Lc^2}{2GI_y} \quad (21)$$

Consequently, displacement field components are:

$$u(x,z) = -\frac{T_z}{2EI_y}\cdot x^2\cdot z + \frac{T_z}{6I_y}\left(\frac{1}{G}-\frac{\upsilon}{E}\right)\cdot z^3 + \frac{T_z L^2}{2EI_y}\cdot z, \quad (22)$$

$$w(x,z) = \frac{\nu T_z}{2EI_y}\cdot x\cdot z^2 + \frac{T_z}{6EI_y}\cdot(x^3-L^3) + \frac{T_z}{2I_y}\cdot\left(\frac{c^2}{G}+\frac{L^2}{E}\right)\cdot(L-x). \quad (23)$$

3. Remarks on Results for the Displacement Field

3.1. Warping of the Cross-Section at the Fixed Support

From Equations 19, 20, 22, and 23, it is evident that the displacements u and w depend on the coordinate z and its exponents, implying warping, known as the cross-section out of plane displacement. Figure 5 shows the horizontal displacement components of several characteristic cross-sections. The following values were used for the plot: load $F = 9\cdot10^{-4}\ GN$, modulus of elasticity $E = 8.5\ GPa$, Poisson's ratio $\nu = 0.35$, section height $h = 2c = 1.8\ m$, and length of girder $L = 3\ m$.

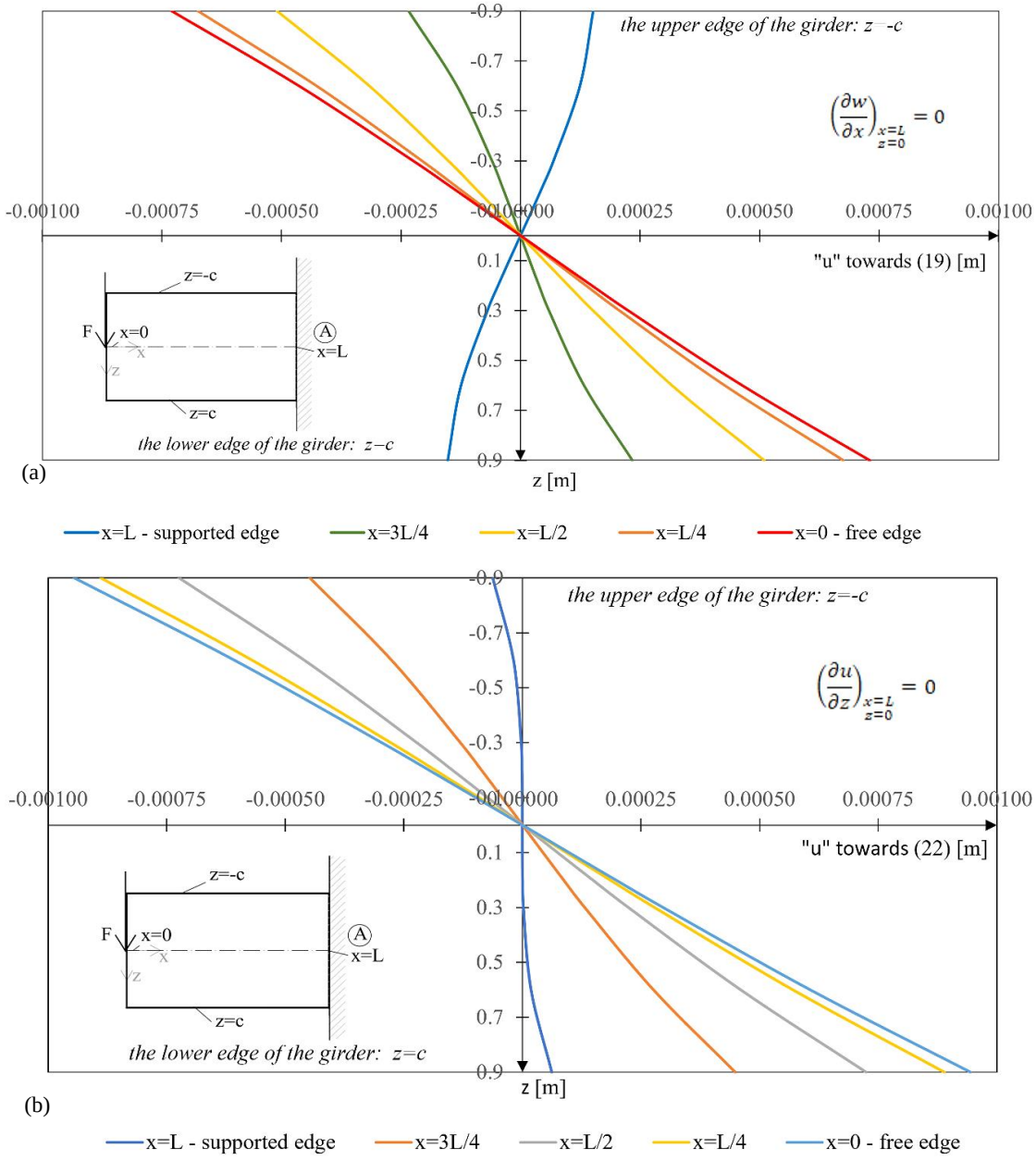

Figure 5. Warping of the cross-sections along the cantilever for different angles of rotation at point A: a) according to Equation 16 and b) according to Equation 17

Because the boundary conditions were defined only for point A and were subject to a certain disturbance, warping occurred at the support (in the vicinity of point A). However, according to St. Venant's principle, the influence of such disturbance decreases with distance; thus, we can accept the solution at the far end of the span (the free end) as sufficiently accurate [4].

Figure 6 shows displacements of points in characteristic sections along the girder corresponding to the two solutions of the displacement field and the input data from the beginning of this section. For better visualization, the horizontal and vertical displacement components were enlarged by a factor of 100.

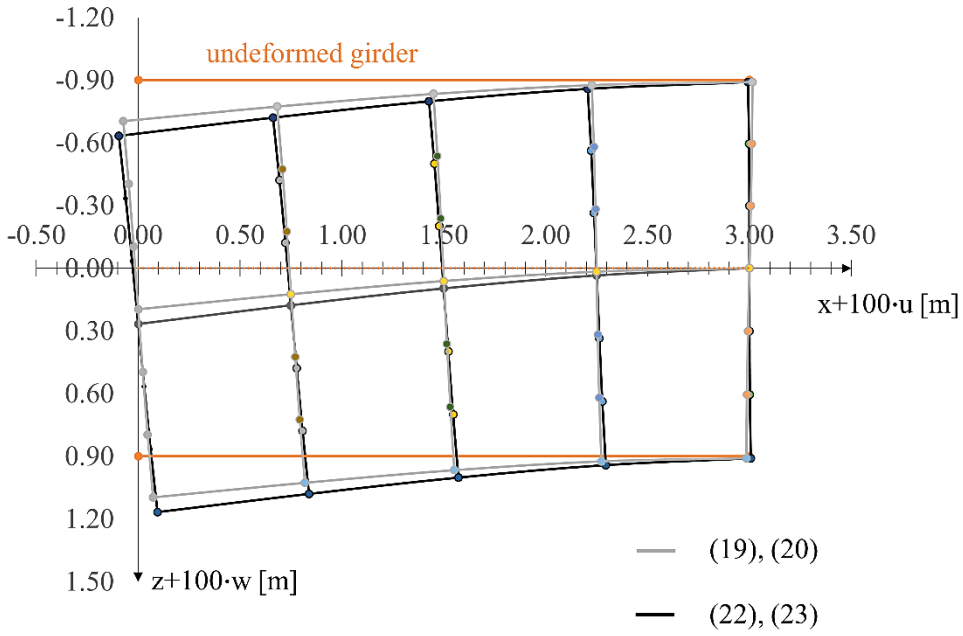

Figure 6. Displacements of points in characteristic sections along the girder

3.2. Axis Deflection

If we extract displacements from the solutions of Equations 19 and 20 only for the axis (at $z = 0$), we obtain:

$$u(x,0) = 0$$
$$w(x,0) = \frac{T_z}{6EI_y} \cdot x^3 - \frac{T_z L^2}{2EI_y} \cdot x + \frac{T_z L^3}{3EI_y} \quad (24)$$

The expression corresponds to the EBN solution for deflection of a slender beam submodel loaded in pure bending obtained under the assumption of infinitely stiff cross-sections perpendicular to the axis (hypothesis of a plane cross-section). Such a solution is also acceptable for concentrated loads when addressing the EBN beams made of common materials ($L/h \geq 5$), [12].

Axis displacements according to the second solution of Equations 22 and 23 are:

$$u(x,0) = 0,$$
$$w = \frac{T_z}{6EI_y} \cdot x^3 - \frac{T_z L^2}{2EI_y} \cdot x + \frac{T_z L^3}{3EI_y} + \frac{T_z c^2}{2GI_y}(L - x). \quad (25)$$

In this case, if compared with Equation (24), the vertical displacement of Equation (25) contains an additional term $T_z\, c^2/(2GI_y) \cdot (L - x)$ that indicates the influence of shear stress on the deflection. Maximum deflection at the free end is expressed as:

$$w = \frac{T_z L^3}{3EI_y} + \frac{T_z c^2}{2GI_y} L. \quad (26)$$

If geometric and material relations $I_y = bh^3/12,\ c = h/2$, and $G = E/[2(1+v)]$ are included in Equation (26) we obtain:

$$w = \frac{T_z L}{Ebh}\left[4\left(\frac{L}{h}\right)^2 + 3(1+v)\right] \quad (27)$$

For different L/h ratios and values of Poisson's ratio, we determined a percentage increase in shear strain deflection (Table 1 and Figure 7).

Table 1. Percentage increase in deflection of free end due to shear strain

Deflection dependence on L/h and υ						
L/h \ υ	0.2	0.25	0.3	0.35	0.4
1	90 %	94 %	98 %	101 %	105 %
2	23 %	23 %	24 %	25 %	26 %
3	10 %	10 %	11 %	11 %	12 %
4	6 %	6 %	6 %	6 %	7 %
5	4 %	4 %	4 %	4 %	4 %

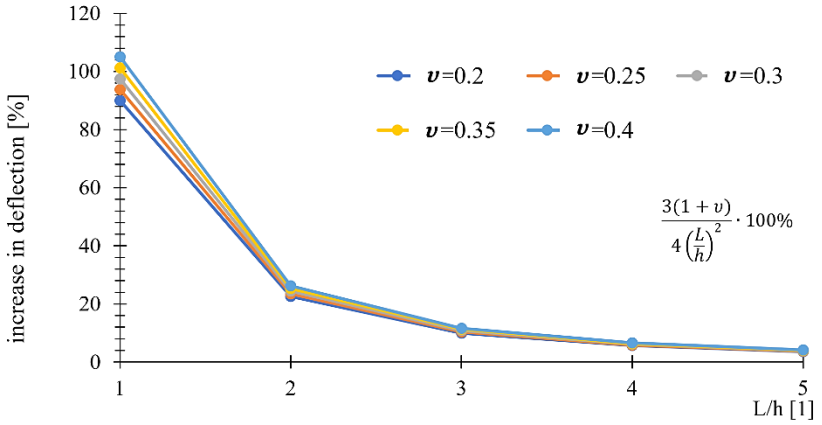

Figure 7. Increase in deflection of Equation 26 due to the contribution of shear strains

The behavior obtained was as expected. The L/h ratio exerted a considerably greater influence than Poisson's ratio. As the length of the girder increased with its height, the influence of the shear stresses on the deflection decreased sharply and fell below 10% for the $L/h \geq 4$. However, for certain materials, a relatively small increase in deflection can result in unfavorable effects. [5].

Therefore, for relatively short and high girders ($L/h < 5$) bent by shear forces, an approximate deflection calculation can be obtained by the Timoshenko beam theory [7].

4. Effect of shear Strain and Approximate Model of a Timoshenko Beam

For the solutions of Equations 19, 20, 22, and 23, the expression for the field of the shear strain is

$$\gamma_{xz} = \frac{\partial u}{\partial z} + \frac{\partial w}{\partial x} = -\frac{T_z}{2GI_y}(c^2 - z^2) \tag{28}$$

It can be concluded that the change in shear strain is owing to the height of the cross-section only. The maximum value of the strain is on the axis and it is $(\gamma_{xz})_{z=0} = -T_z\, c^2/(2GI_y)$, while it is zero at the edges of the girder $(\gamma_{xz})_{z=\pm c} = 0$. Thus, the tangents of the upper and lower edges of the girder are perpendicular to the tangent of the deformed cross-section, whereas at the axis of the girder, the angle between the tangent to the axis and the cross-section deviates from the right angle (Figure 8-a). Therefore, the strains and stresses are in accordance with the analytical solution; thus, in addition to the equilibrium equations, the compatibility conditions are also satisfied.

Contrary to the analytical solution, the assumption of a rigid cross-section perpendicular to the beam deflection introduced by EBN for pure bending neglects the compatibility of displacement when the beam is loaded with shear forces. On the axis of the beam, at the location of the maximum shear stresses (determined from the equilibrium conditions), the differential element has right angles. Consequently, the axis is free of shear strains (Figure 8b).

A solution that slightly improves the displacement incompatibility of the EBN beam is the Timoshenko beam [7]. The calculation retains the assumption that the cross-sections remain rigid but can be rotated relative to the beam axis (Figure 8c). However, this solution also "suffers" from displacement incompatibility because the right angle at the upper or lower edge of the beam is not maintained.

4.1. Timoshenko Beam

Deflection according to the Timoshenko beam theory is an approximate solution of the girder axis, wherein a pure shear term w_τ is added to the deflection according to pure bending (EBN solution). As differential elements of the girder on the neutral axis are only subjected to the shear stresses (pure shear), it is assumed that the elements remain vertical and slide relative to each other (Figure 9).

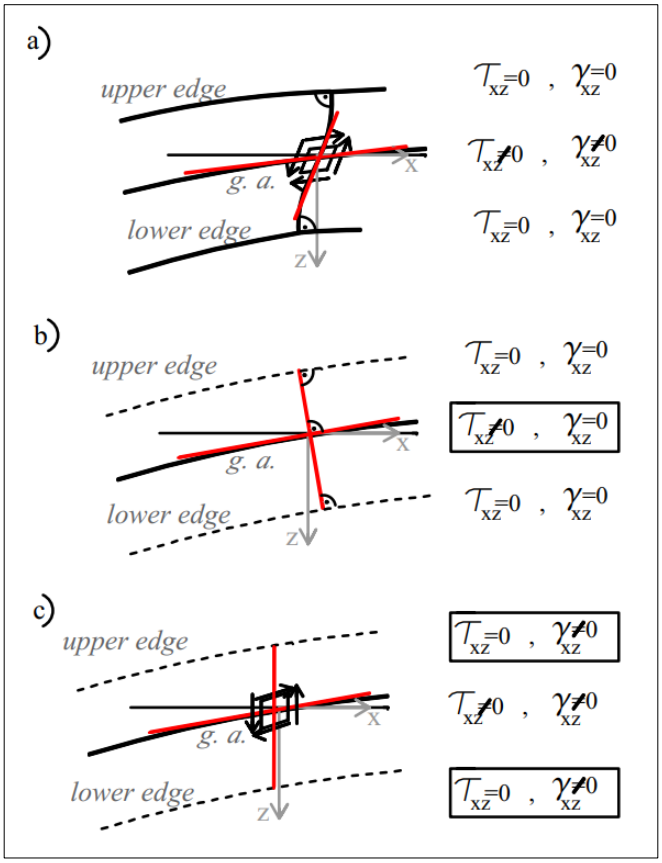

Figure 8. Scheme of shear stresses and strains for different assumptions: a) analytical solutions of Equations 19 and 20 or 22 and 23, b) EBN beam, and c) Timoshenko beam

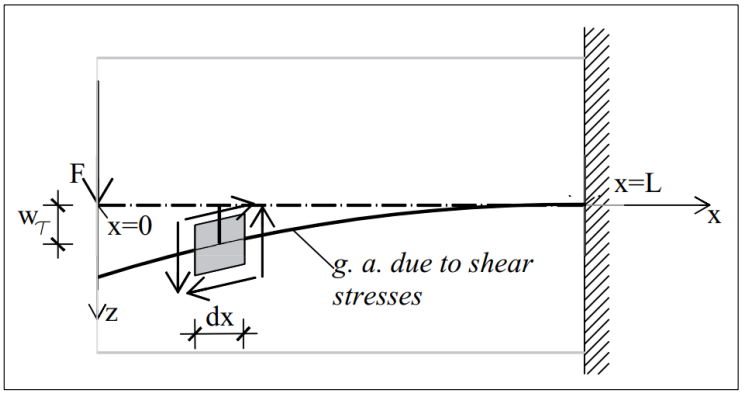

Figure 9. A differential element on the neutral axis of the girder under shear stresses

The slope of the tangent to the deflection line (caused only by shear stresses) corresponds to the shear angle as follows:

$$\frac{dw_\tau}{dx} = (\gamma_{xz})_{z=0} = \frac{(\tau_{xz})_{z=0}}{G} = -\frac{T_z S_y}{I_y b G} = -\frac{T_z}{2I_y G} c^2 \quad (29)$$

where the static moment for half of the rectangular section is $S_y = bh^2/8$, and for h =2c, b =1 yields $S_y = c^2/2$.

The geometrical boundary condition where rotational degree of freedom at the support point is fixed, $(dw_\tau/dx)_{x=L} = 0$, yields from Equation 29:

$$w_\tau = \frac{T_z}{2I_y G} c^2 (L - x) \quad (30)$$

Equation 30 and the deflection of the free end $w_\tau = T_z\, c^2/(2GI_y) \cdot L$ correspond to the additional terms in Equations 25 and 26. Although the solution for the Timoshenko beam is consistent with the analytical solution (on the girder axis), the calculation is considered approximate because it does not provide exact solutions outside the axis. The solution retains the rigidity of the cross-section, implying that the compatibility conditions at the upper and lower edges are not satisfied.

5. Numerical Solution

The numerical calculations were performed using the structural analysis program SAP2000. Four basic numerical models were selected: beam models with and without the influence of shear strains on the deflection (EBN and Timoshenko beams), two-dimensional (2D) models with quadrilateral plane stress elements, and three-dimensional (3D) models with eight-node brick elements.

Beam models M1 and M2 (Table 2) are included in a single element formulation because such formulations fully capture the result. The load was applied as a concentrated force and the support point is clamped.

Table 2. Basic data on numerical models

Model label	Finite element	Model with load and boundary conditions
M1	EBN beam element	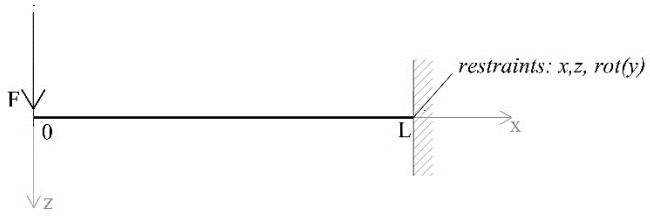
M2	Timoshenko beam element	
M3a	Quadrilateral plane stress element	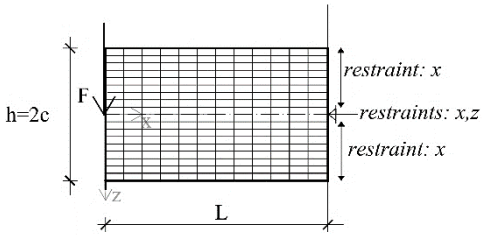 $F = \int_{-c}^{c} q_f \, dz$
M3b		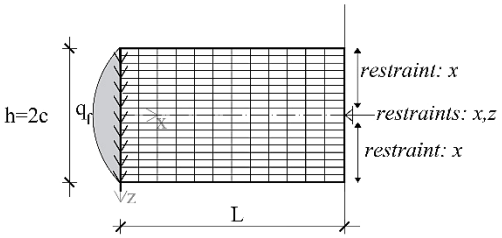
M4a	Eight-nodded brick element	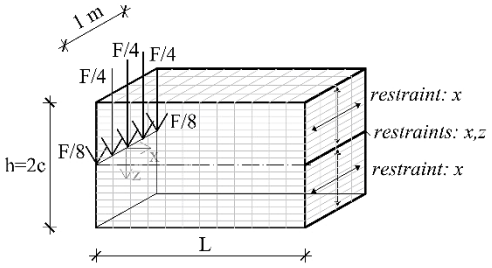 $F = \iint_A q_f \, dydz, \; A = [-c, c] \times [-0.5, 0.5]$
M4b		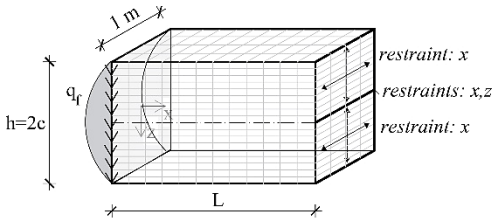

Model M3 was discretized with $12 \times 18 = 216$ elements with an aspect ratio of 2.5: 1. There were 474 degrees of freedom. Model M4 had $12 \times 18 \times 4 = 864$ elements with ratios of 2.5: 1: 2.5 and 3610 degrees of freedom. The boundary conditions of the model based on the displacements are listed in Table 2.

The plane and spatial models were calculated for two types of loading: the concentrated resultant force F acting on the axis of model M3a, that is along the neutral plane of model M4a, and the continuous tangential load q_f with a parabolic distribution over the height or surface of models M3b and M4b. The continuous load is discretized on the nodes of the element and is equal to force F.

The values listed in Section 3.1 were used for comparing the results:

$F = 9 \cdot 10^{-4}\ GN$, $E = 8.5\ GPa$, $\nu = 0.35$, $h = 2c = 1.8\ m$ and $L = 3\ m$.

6. A Comparison of Results

Figure 10 shows the deformed shapes of all numerical models. The displacements of beams 10a), 2D model 10b), and 3D model 10c) were compared.

(a) M1 and M2

M1:
$u = 0\ m$, $w_{max} = 0.001961\ m$

M2:
$u = 0\ m$, $w_{max} = 0.002533\ m$
RDu: 0% RDw: -22.6%

(b) M3a and M4a

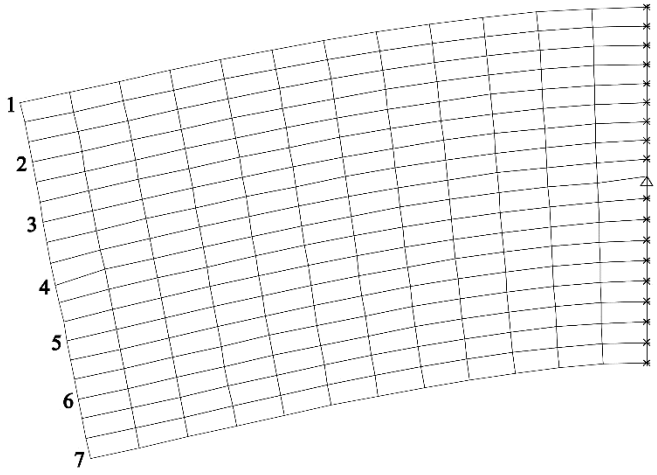

4

M3a:
$u = 0\ m;\ w_{max} = 0.002769\ m$

M4a:
$u = 0\ m;\ w_{max} = 0.002752\ m$

7

M3a:
$u_{max} = 0.000888\ m;$
$w_{max} = 0.002625\ m$

M4a:
$u_{max} = 0.000889\ m;$
$w_{max} = 0.002614\ m$

	RDu [%]	RDw [%]
1	-0.1	0.4
2	0.0	0.3
3	1.7	0.2
4	0.0	0.6
5	1.7	0.2
6	0.0	0.3
7	-0.1	0.4

(c) M3b and M4b

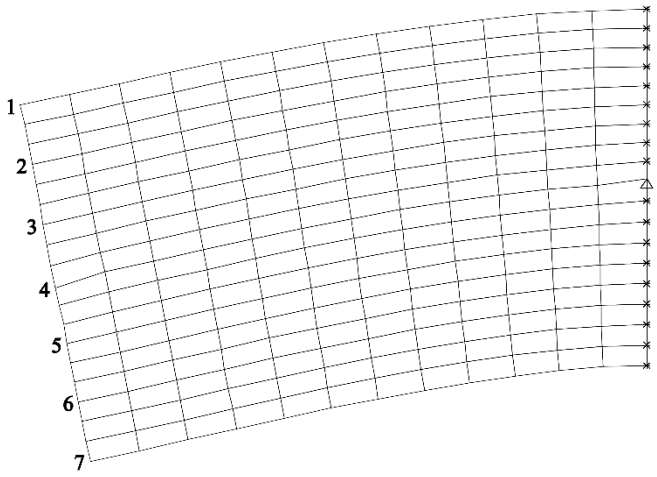

4

M3b:
$u = 0\ m;\ w_{max} = 0.002666\ m$

M4b: $u = 0\ m;\ w_{max} = 0.002658\ m$

7

M3b:
$u_{max} = -0.000912\ m;$
$w_{max} = 0.002666\ m$

M4b:
$u_{max} = 0.000915\ m;$
$w_{max} = 0.002658\ m$

	RDu [%]	RDw [%]
1	-0.1	0.4
2	0.0	0.3
3	1.7	0.2
4	0.0	0.6
5	1.7	0.2
6	0.0	0.3
7	-0.1	0.4

Figure 10. Deformed shape of all numerical models

For the free end ($x = 0$), the differences in the horizontal (RDu) and vertical (RDw) displacements are compared for the following models: M1 to M2, M3a to M4a, and M3b to M4b (Figure 10).

Table 3. Differences of horizontal and vertical displacements of analytical solution A1 and numerical solutions M1, M2, M3a, M3b, M4a compared to analytical solution A2 for the free end of the girder (x=0)

	A1		M1		M2		M3a		M3b		M4a		M4b	
z [m]	RDu [%]	RDw [%]	RDu [%]	RDw [%]	RDu [%]	RDw [%]	RDu [%]	RDw [%]	RDu [%]	RDw [%]	RDu [%]	RDw [%]	RDu [%]	RDw [%]
-0.9	-22.8	-26.7	-	-	-	-	-6.0	-1.9	-3.5	-0.3	-5.9	-2.3	-3.2	-0.6
-0.6	-23.6	-26.7	-	-	-	-	-3.8	-1.8	-3.6	-0.3	-3.8	-2.1	-3.3	-0.6
-0.3	-24.0	-26.7	-	-	-	-	1.0	-0.8	-3.4	-0.3	-0.7	-1.0	-3.0	-0.6
0.0	0.0	-26.7	0.0	-26.7	0.0	-5.3	0.0	3.5	0.0	-0.3	0.0	2.9	0.0	-0.6
0.3	-24.0	-26.7	-	-	-	-	1.0	-0.8	-3.4	-0.3	-0.7	-1.0	-3.0	-0.6
0.6	-23.6	-26.7	-	-	-	-	-3.8	-1.8	-3.6	-0.3	-3.8	-2.1	-3.3	-0.6
0.9	-22.8	-26.7	-	-	-	-	-6.0	-1.9	-3.5	-0.3	-5.9	-2.3	-3.2	-0.6

The expected results were achieved. The biggest difference was obtained between the beam models (22.6%), while the differences in the displacement components of the planar and spatial models loaded with a continuous or equivalent concentrated load were very small (0.0 – 1.7%). For the free end ($x = 0$), Table 3 shows the differences in RDu and RDw of the analytical solution A1 [Equations 19 and 20] and numerical solutions M1, M2, M3a, M3b, M4a, and M4b when compared to analytical solution A2 [Equations 22 and 23].

As evidenced by the results above, displacements of numerical models M2, M3a, M3b, M4a, and M4b and analytical solution A2 are similar, differences are in the range of 0.0–6.0%. Numerical models behaved more rigidly (negative relative differences, i.e., smaller displacement values), which corresponds to the classical, displacement-based definition of finite elements [22, 23]. Only models M3a and M4a exhibited larger displacements near the girder axis compared to the displacements determined using analytical method A2, which is a consequence of the position of the concentrated force in these models. The smallest differences were found for models M3b and M4b, with the parabolic external load, which is expected.

However, for models M1 and A1 the results on the axis are consistent. The relative difference in the displacement of A1 and M1 when compared to A2 is significant 26.7 %. Figure 11 shows the warping of the free cross-section (x= 0) for A1, A2, M3a, M3b, M4a, and M4b. Satisfactory agreement between M3a, M3b, M4a, and M4b and A2 is observed.

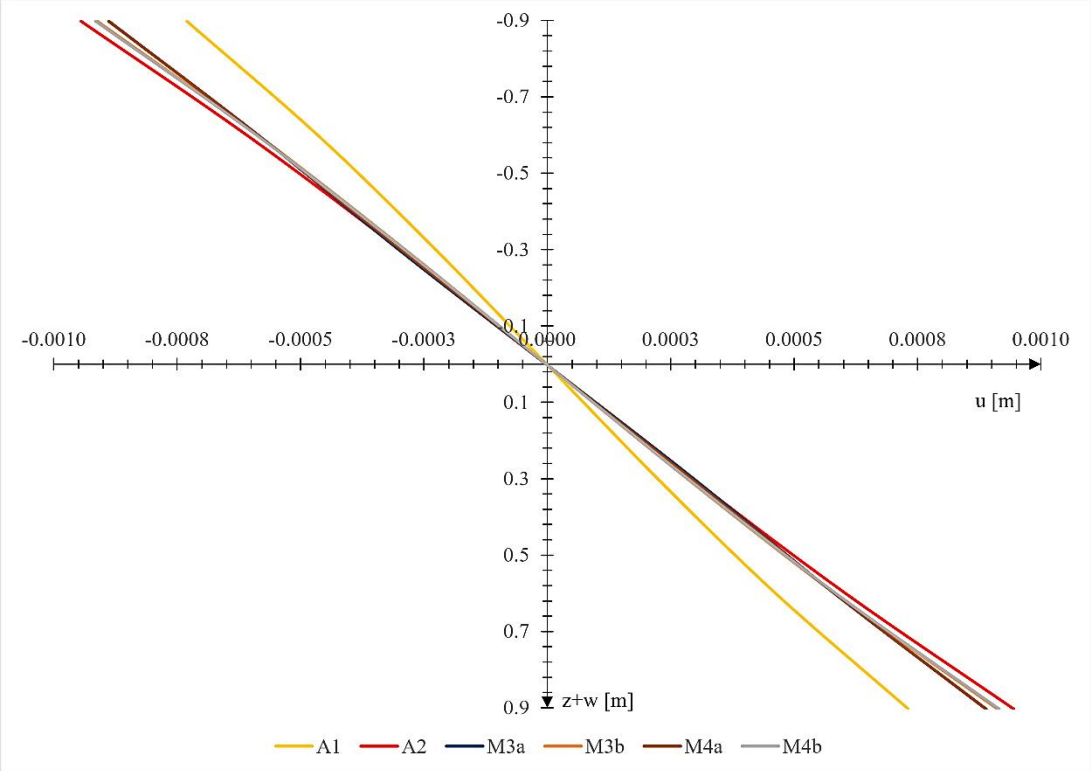

Figure 11. Warping of the free cross-section (x=0)

7. Conclusions

For the cantilever with rectangular cross-section and load at the tip it can be concluded:

- When defining the analytical solution for the boundary value problem this study has shown that the maximum values of the displacement field were obtained for $u(L,0)=0$, $w(L,0)=0$ and $(\partial u/\partial z)_{x=L,z=0}=0$ (analytical solution A2).
- By comparing analytical and numerical solutions, the largest differences were expected for the EBN beam because it is a submodel for which the equilibrium and compatibility conditions are not in agreement. Assumption about rigid and perpendicular cross sections makes displacements significantly smaller. The Timoshenko beam causes a better agreement among the results because it relaxes the assumption about the rotation of the rigid cross-sections and thus decreases displacement incompatibility.
- The results of 2D models with quadrilateral plane stress elements or 3D models with eight-nodded brick elements are the closest to the analytical solutions A2.
- Equation 27 which can be simplified as $w = const \cdot [4(L/h)^2 + 3(1+\upsilon)]$ is generally valid. Overall results confirm that the increase in deflection was primarily dependent on the ratio L/h, not on the E and cross-sectional constants. Also, for L/h=1 the shear force caused almost the same deflection as pure bending. Additionally, the influence of Poisson's ratio was not significant for standard materials like wood, steel or concrete.

The main limitation of the plane stress problem is the assumption about linear stress distribution along the cross-section. This is approximately accurate, but only for relatively thin girders. In future work, other stress distributions that are more appropriate for deep girders should be adopted. In such cases, searching for analytical or semi-analytical solutions could be challenging, although research should be made much easier using programs like Wolfram Mathematica or MATLAB. This strategy can offer clear explanations, interpretations, and limitations of the background theory and useful practical benchmarks.

8. Nomenclature

A	Cross-sectional area, m^2	$a_2, a_4, b_2, b_4, c_4, d_4, e_4$	Constants of second and fourth-degree polynomials
b	Cross-sectional width, m	c	Half height of the cross-section, m
d, e, f, g	Constants of integration	E	Modulus of elasticity, N/m^2
F	Concentrated force, N	G	Shear modulus, N/m^2
h	Cross-sectional height, m	I_y	Moment of inertia, m^4
L	Girder length, m	M	Reaction (moment), Nm
M_y	Bending moment, Nm	$p_1(z), p_2(x)$	Functions of one variable
q_f	Continuous tangential parabolic loading over the height (N/m) or surface (N/m^2)	R	Reaction (force), N
RDu	Relative difference in the horizontal displacements	RDw	Relative difference in the vertical displacements
S_y	Static moment of area, m^3	T_z	Shear force, N
T	Centroid of a girder cross-section	u	Horizontal displacement, m
w	Vertical displacement, deflection, m	w_τ	Shear deflection, m
x, y, z	Axes of the right Cartesian coordinate system	γ_{xz}	Shear strain
$\varepsilon_x, \varepsilon_y, \varepsilon_z$	Normal strain components	ν	Poisson's ratio
σ_x, σ_z	Normal stress components, N/m^2	τ_{xz}, τ_{zx}	Shear stress components, N/m^2
$\Phi\ (x,z)$	Stress function	$\Phi_2(x,z), \Phi_4(x,z)$	Second and fourth-degree polynomials with two variables

9. Declarations

9.1. Author Contributions

Conceptualization, A.J.L. and T.M.; methodology, A.J.L. and T.M.; software, A.J.L. and T.M.; validation, A.J.L. and T.M.; formal analysis, A.J.L. and T.M.; investigation, A.J.L.; resources, E.Š. and E.J.; data curation, A.J.L., T.M., E.Š., and E.J.; writing—original draft preparation, A.J.L. and T.M.; writing—review and editing, A.J.L., T.M., E.Š., and E.J.; visualization, T.Š. and E.J.; supervision, T.M. and E.Š. All authors have read and agreed to the published version of the manuscript.

9.2. Data Availability Statement

The data presented in this study are available upon request from the corresponding author.

9.3. Funding

The authors received no financial support for the research, authorship, and/or publication of this article.

9.4. Conflicts of Interest

The authors declare no conflict of interest.

10. References

[1] Byskov, E. (2013). Elementary Continuum Mechanics for Everyone. In Solid Mechanics and Its Applications. Springer, Dordrecht, Netherlands. doi:10.1007/978-94-007-5766-0.

[2] Slaughter, W. S. (2002). The Linearized Theory of Elasticity. Birkhäuser Boston, Boston, United States. doi:10.1007/978-1-4612-0093-2.

[3] Dvornik, J., & Lazarević, D. (2007). The Role of Creativity and Engineering Judgment in Construction Work. Građevinar, 59(03), 197-207.

[4] Timoshenko, S., & Goodier, J. N. (1951). Theory of elasticity. McGraw-Hill Book, New York, United States.

[5] Hjelmstad, K. D. (2007). Fundamentals of structural mechanics. Springer Science & Business Media, New York, United States.

[6] Dvornik, J., Lazarević, D., & Bićanić, N. (2019). On the principles and procedures of budgeting of building structures. Faculty of Civil Engineering, University of Zagreb, Zagreb, Croatia. doi:10.5592/bo/2019.978-953-8168-31-4.

[7] Ibrahimbegovic, A., & Mejia-Nava, R.-A. (2023). Structural Engineering. In Lecture Notes in Applied and Computational Mechanics. Springer International Publishing, Cham, Switzerland. doi:10.1007/978-3-031-23592-4.

[8] R. Eugster, S. (2015). Geometric Continuum Mechanics and Induced Beam Theories. In Lecture Notes in Applied and Computational Mechanics. Springer International Publishing, Cham, Switzerland. doi:10.1007/978-3-319-16495-3.

[9] Goldberg, D. (1991). What every computer scientist should know about floating-point arithmetic. ACM Computing Surveys (CSUR), 23(1), 5–48. doi:10.1145/103162.103163.

[10] Dvornik, J., & Lazarević, D. (2005). Shortcomings of Calculation Models of Engineering Structures. Građevinar, 57(04.), 227-236.

[11] Bathe, K. J. (1996). Finite element procedures. Prentice Hall, New Jersey, United States.

[12] Öchsner, A. (2021). Classical Beam Theories of Structural Mechanics. Springer International Publishing, Cham, Switzerland. doi:10.1007/978-3-030-76035-9.

[13] Obert, L., & Duvall, W. I. (1967). Rock mechanics and the design of structures in rock. John Wiley and Sons, Hoboken, United States.

[14] Ahmed, A. M., & M. Rifai, A. (2021). Euler-Bernoulli and Timoshenko Beam Theories Analytical and Numerical Comprehensive Revision. European Journal of Engineering and Technology Research, 6(7), 20–32. doi:10.24018/ejeng.2021.6.7.2626.

[15] Rahmani, F., Kamgar, R., & Rahgozar, R. (2020). Finite element analysis of functionally graded beams using different beam theories. Civil Engineering Journal (Iran), 6(11), 2086–2102. doi:10.28991/cej-2020-03091604.

[16] Gaur, A., & Dhurvey, P. (2020). Comparative Study of Beam Theories on the Effect of Span-Depth Ratio for Symmetric and Un-symmetric Loadings. IOP Conference Series: Materials Science and Engineering, 936(1), 012047. doi:10.1088/1757-899X/936/1/012047.

[17] Zhang, G. Y., & Gao, X. L. (2020). A new Bernoulli–Euler beam model based on a reformulated strain gradient elasticity theory. Mathematics and Mechanics of Solids, 25(3), 630–643. doi:10.1177/1081286519886003.

[18] Perez-Garcia, C., Aranda-Ruiz, J., Zaera, R., & Garcia-Gonzalez, D. (2022). Beam formulation and FE framework for architected structures under finite deformations. European Journal of Mechanics, A/Solids, 96. doi:10.1016/j.euromechsol.2022.104706.

[19] Yawei, D., Yang, Z., & Jianwei, Y. (2020). Exact solutions of bending deflection for single-walled BNNTs based on the classical Euler-Bernoulli beam theory. Nanotechnology Reviews, 9(1), 961–970. doi:10.1515/ntrev-2020-0075.

[20] Alavi, S. E., Sadighi, M., Pazhooh, M. D., & Ganghoffer, J. F. (2020). Development of size-dependent consistent couple stress theory of Timoshenko beams. Applied Mathematical Modelling, 79, 685–712. doi:10.1016/j.apm.2019.10.058.

[21] Franza, A., Acikgoz, S., & DeJong, M. J. (2020). Timoshenko beam models for the coupled analysis of building response to tunnelling. Tunnelling and Underground Space Technology, 96. doi:10.1016/j.tust.2019.103160.

[22] Davari, S. M., Malekinejad, M., & Rahgozar, R. (2019). Static analysis of tall buildings based on Timoshenko beam theory. International Journal of Advanced Structural Engineering, 11(4), 455–461. doi:10.1007/s40091-019-00245-7.